Royal Institute of Technology, 100 44 Stockholm, Sweden
Mechatronics basic course MF2030
Wednesday 30th October, 2024
Hsiu-Fang Chien 19970515-R083
Johan Kindlundh 20000715-8231
Vittoria Charrère 20011220-T207

Analysis and design of an electric nut runner for tightening of bolted joints

Contents

Introduction

This project focuses on learning how to solve a mechatronics problem through a model-based approach. The process begins with conceptualizing the system with subsystems for further analysis and component selection. By modelling and simulating the system with different methods and levels of detail, we can predict how the nut runner behaves under different conditions. These models are the basis for developing control systems for optimal performance. The system's behaviour was verified to ensure it meets the desired specifications.
This report documents our approach to the analysis and design of the electric nutrunner. It also demonstrates the practical application of a model-based method in addressing a mechatronics design problem.

Modeling and assumptions

System to be designed

The system under consideration in this project is cordless (battery-powered) Tensor ITB-A61-50-10 nutrunner. The components of the nutrunner include a basic cylinder-shaped mechanical structure, a battery, a brushless DC-motor, a two-stage planetary gear, a torque transducer, a 90-degree spiral angle gear, an operator interface, a communication interface, a one-piece angle head, and a handle. The technical specifications for the nutrunner are shown in Table 1.

Property	**Value**
Torque Max/Min (Nm)	55/10
Maximum speed (rpm)	587
Weight (kg)	2.5 with battery
Motor power (W)	1500

Table 1: Technical specifications: ITB-A61-50-10

The motor assigned for this assignment is 4490 024 B, with its specifications in Table 2.

Property	**Value**
Nominal torque (mNm)	190
Terminal resistance, phase-phase (Ohm)	0.22
Friction torque, dynamic (mNm/min^{-1})	$7.72 \cdot 10^{-4}$
Back-EMF constant (mV/min^{-1})	2.53
Torque constant (mNm/A)	24.2
Terminal inductance, phase-phase (μH)	73
Rotor inertia (gcm^2)	130

Table 2: Motor Specifications: 4490 024 B

Initial assumptions

- The 4490 024 B motor is modelled as DC-motor equivalents for simplification. The equivalent DC-current is provided in Faulhaber datasheet.
- The socket to fit the nut is stiffly connected with a tight fit, allowing us to consider the tool chassis rotation to be in the horizontal plane only.
- The battery's mass centre is at r-coordinate of 500 mm. The tool's mass centre (excluding the battery) is at r-coordinate of 250 mm.
- The tightening process only includes the rundown and elastic phases. The nutrunner does not run continuously, allowing a design utilizing the motor's stall torque.
- The transmission ratio of the 90-degree angle gear is 1. The transmission is considered to have no losses.
- Lumped parameters and linear models can be used.
- All mechanical interconnections except the planetary gear stages are considered as infinitely stiff.

- System damping comes from DC-motor resistance, the linear friction in the nut, and the friction in the tool.
- The angle gear, output and input shafts are considered rigid.
- All transmission components are made of steel.
- The flexibility in the transmission is confined to two planetary gear stages and equals in total $k_t = 739Nm/rad$ as estimated on the output side of the planetary gear pair.
- The transmission damping is linear, equals to $d_t = 1.5Nm \cdot s/rad$ as estimated on the output side of the planetary gear pair, and is considered relative.
- The joint friction in the screw/nut assembly is assumed linear, equals $d_j = 1.5Nm \cdot s/rad$ and is considered absolute.
- The longitudinal stiffness of the steel screw k_j is calculated from dimensions and material properties, with no torsional twist.

1 Task 1

1.1 Differential equations

The electrical behavior of the DC motor can be described by Kirchhoff's voltage law. The voltages include the resistive drop, the inductive effect from the motor's coil and the back EMF as shown in Equation (1).

$$V(t) = Ri(t) + L\frac{di(t)}{dt} + K_e\omega(t) \tag{1}$$

where: R is the resistance, i is the current, L is the inductance, K_e is the back EMF constant, and ω is the angular velocity.

The mechanical dynamics can be described by Newton's second law. The applied net torque is equal to the product of its inertia and angular acceleration as shown in Equation (2).

$$J\frac{d\omega(t)}{dt} = K_m i(t) - frT\omega(t) \tag{2}$$

where: J is the inertia, K_m is the torque constant, and frT is the dynamic friction torque.

1.2 Block diagram (Simulink)

The block diagram, as shown in Figure 1, represents integrated electrical and mechanical dynamics. The model is constructed in Simulink and shows how the components interact.

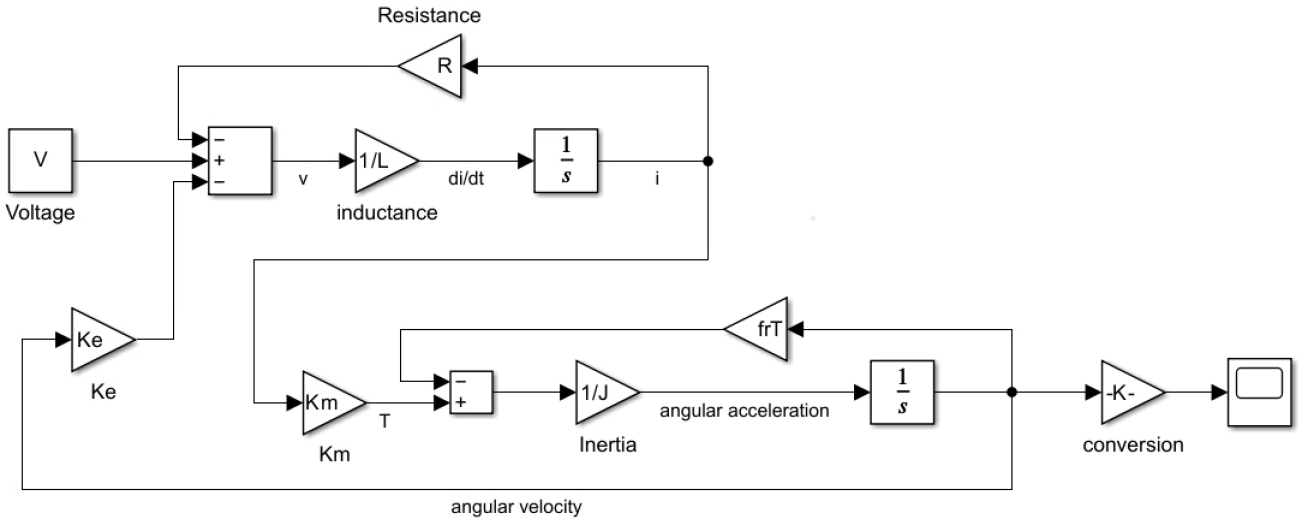

Figure 1: Block diagram

1.3 State-space model (MATLAB and Simulink)

To reformulate Equations (1) and (2) into a state-space model, Our variables of interest are as Equation (3). X is the state, u is the input variable, and Y is the output variable.

$$X = \begin{bmatrix} X_1 \\ X_2 \end{bmatrix} = \begin{bmatrix} \omega \\ i \end{bmatrix}, \quad u = V, \quad Y = \omega \tag{3}$$

The state-space representation is given by Equation (4) and (5).

$$\dot{X} = AX + Bu \tag{4}$$

$$Y = CX + Du \tag{5}$$

where system matrices are derived as Equation (6).

$$A = \begin{bmatrix} -\frac{\mathrm{frT}}{J} & \frac{K_m}{J} \\ -\frac{K_e}{L} & -\frac{R}{L} \end{bmatrix}, \quad B = \begin{bmatrix} 0 \\ \frac{1}{L} \end{bmatrix}, \quad C = \begin{bmatrix} 1 & 0 \end{bmatrix}, \quad D = 0 \tag{6}$$

With the matrices, the state-space model can be symbolically represented in Matlab as Figure 2.

```
A = [-frT/J Km/J; -Ke/L -R/L];
B = [0; 1/L];
C = [1 0];
D = 0;

sys_ss = ss(A,B,C,D);
```

Figure 2: State-space model in Matlab

In Simulink, the state-space block was applied to implement the system as shown in Figure 3.

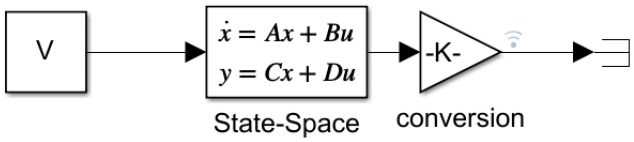

Figure 3: State-space model in Simulink

1.4 Transfer functions model (MATLAB and Simulink)

Given Equation (1) and (2), Laplace transform are applied to transfer from time domain to frequency domain, assuming zero initial conditions for current $i(0) = 0$ and for angular velocity $\omega(0) = 0$. First, by applying Laplace transform to the electrical dynamic Equation (1), we get Equation (7).

$$LsI(s) = -RI(s) + V(s) - k_e\Omega(s) \tag{7}$$

By rearranging the terms, we obtain the isolate Laplace transform of the current i as Equation 8.

$$I(s) = \frac{V(s) - k_e\Omega(s)}{(Ls + R)} \tag{8}$$

Same with Equation (2), applying Laplace transform results in equation (9).

$$Js\Omega(s) = k_m I(s) - frT\Omega(s) \tag{9}$$

By rearranging the terms, we obtain Laplace transform of angular velocity ω as Equation (10).

$$\Omega(s) = \frac{K_m I(s)}{(Js + frT)} \tag{10}$$

By substituting $I(s)$ from Equation (8) into Equation (10) and rearranging the terms, we find the transfer function that relates the output angular velocity to the input voltage as Equation (11).

$$\frac{\Omega(s)}{V(s)} = \frac{k_m}{(Js + frT)(Ls + R) + K_m k_e} \tag{11}$$

The derived transfer function can be symbolically represented in Matlab as Figure 4.

```
num = Km;
den = [J*L (J*R+frT*L) (Km*Ke+R*frT)];

sys_tf = tf(num,den);
```

Figure 4: Transfer function model on Matlab

In Simulink, we utilize the transfer function block to implement the model as shown in 5.

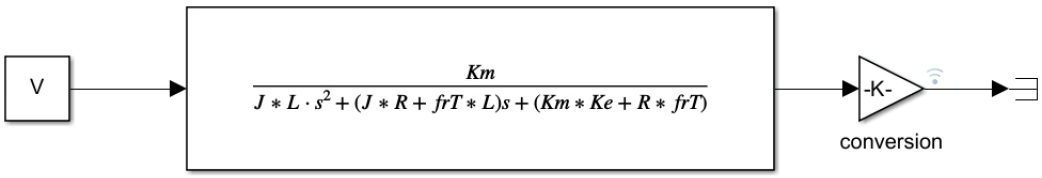

Figure 5: Transfer function model in Simulink

1.5 Multidomain physical model (Simscape)

A multidomain physical model is created in Simscape as in Figure 6.

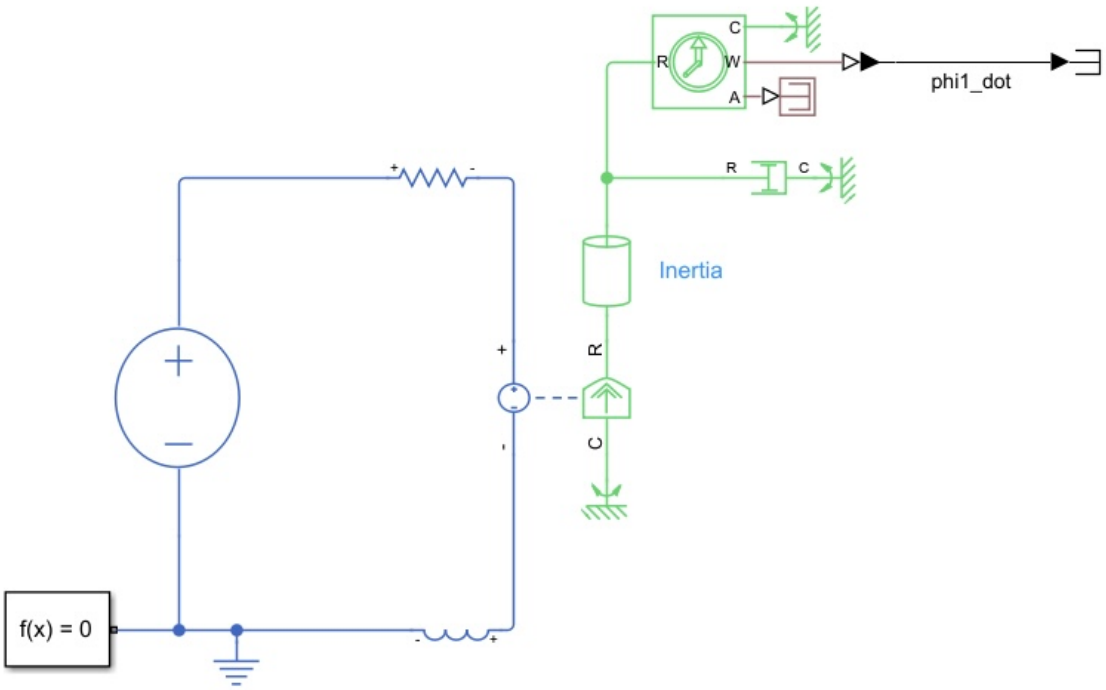

Figure 6: Multidomain model on Simscape

1.6 Result of the Models

The parameters are defined in MATLAB based on the given data sheet (see Appendix):

$$K_e = 2.53 \times 10^{-3} \times \frac{60}{2\pi} \frac{V}{rad/s}$$

$$K_m = 24.2 \times 10^{-3}\ Nm/A$$

$$L = 73 \times 10^{-6}\ H$$

$$R = 0.22\ \Omega$$

$$V = 24\ V$$

$$J = 130 \times 10^{-7}\ kgm^2$$

$$frT = 7.72 \times 10^{-7} \times \frac{60}{2\pi} \frac{Nm}{rad/s}$$

The different models are then compared with the same input. The angular velocity of all models performs the same as in Figure 7.

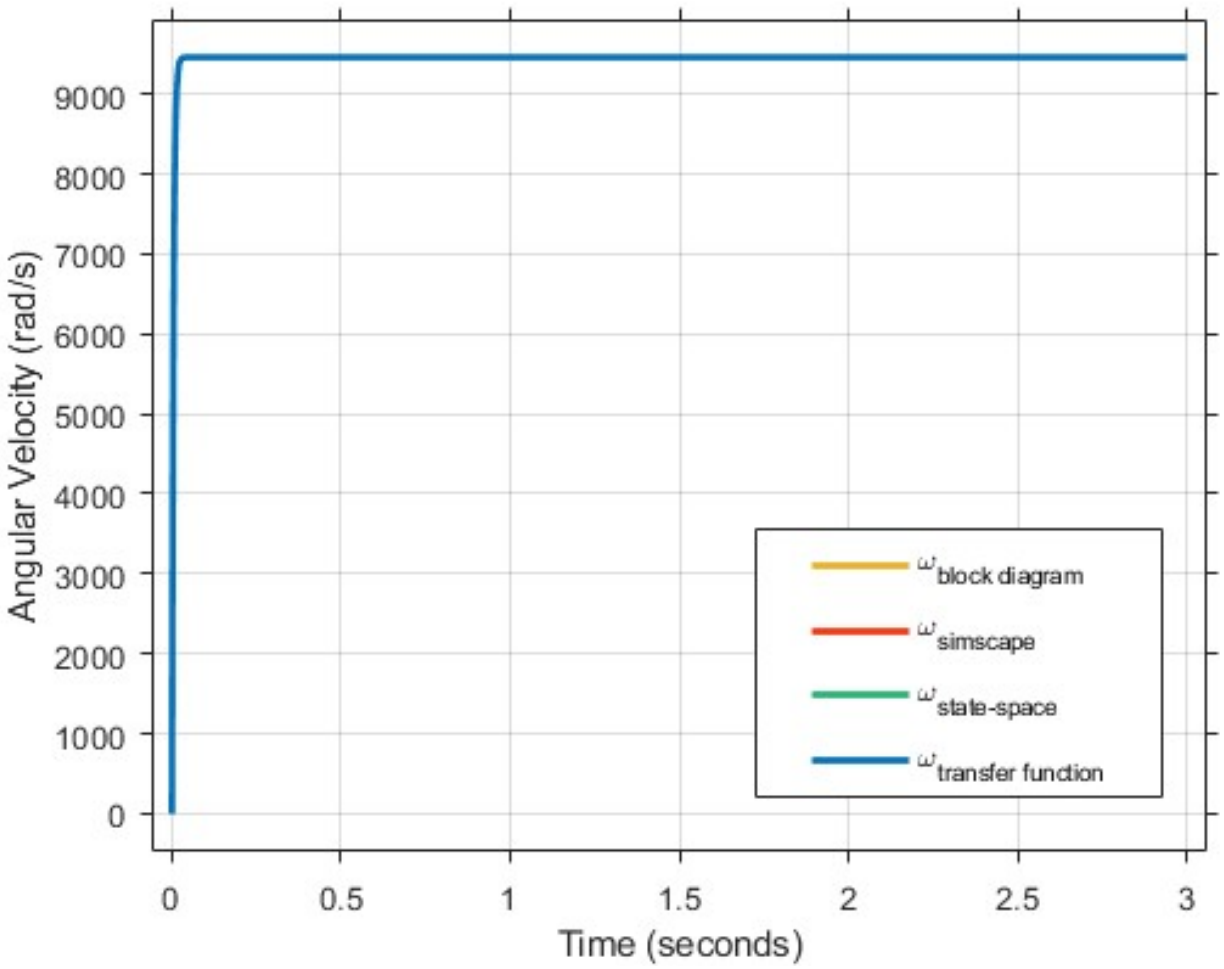

Figure 7: Results of ω based on different models

2 Task 2

The aim of this section is to verify by simulation that the models of the DC motor previously created are in fact working as intended. A voltage step of $V = 24\ V$ is applied as an input to the models, the response in the time-domain in terms of current, angular acceleration and angular velocity is analyzed and compared to the motor's data sheet (see Appendix).

2.1 Current i

Current is compared to no-load current $i_0 = 0.527\ A$

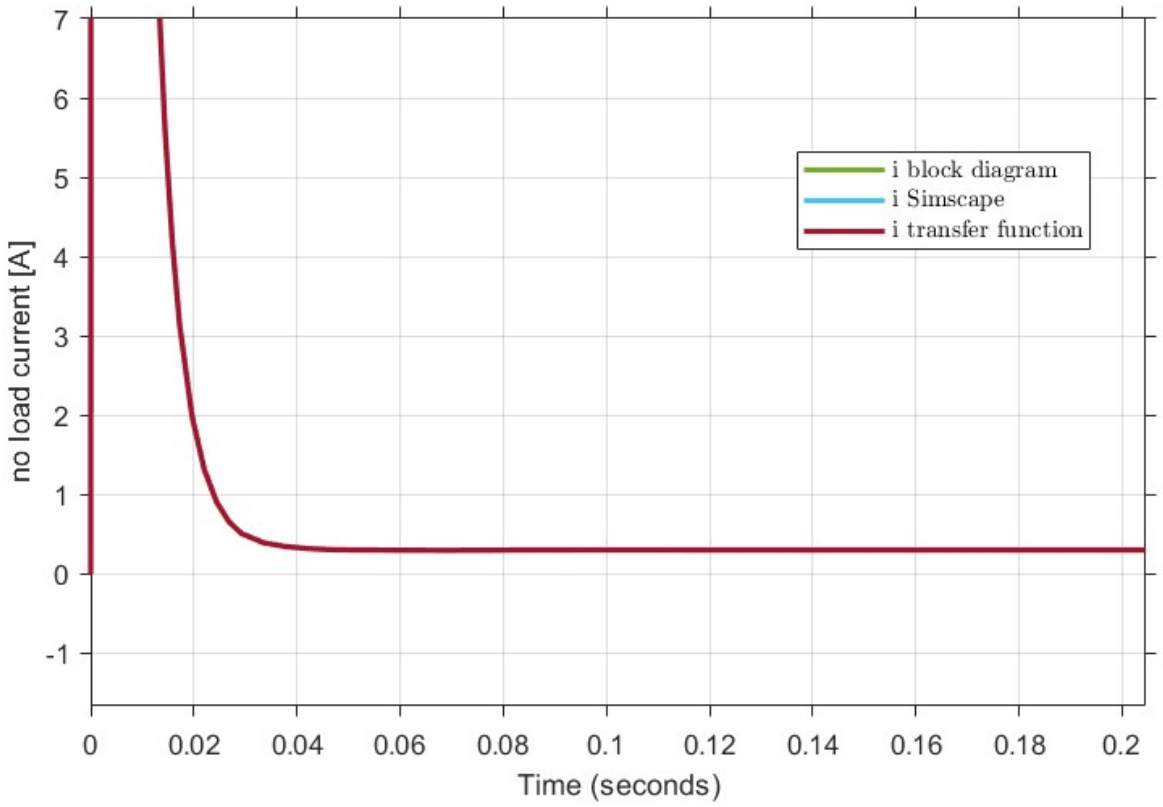

Figure 8: Verification of the models: no-load current i_0

Figure 8 shows that at steady state and with no external load the current reflects the predicted data sheet current fairly well with a value of $0.456A$.

2.2 Angular acceleration $\dot{\omega}$

Compare to angular acceleration max $\alpha_{max} = 203 * 10^3\ rad/s^2$

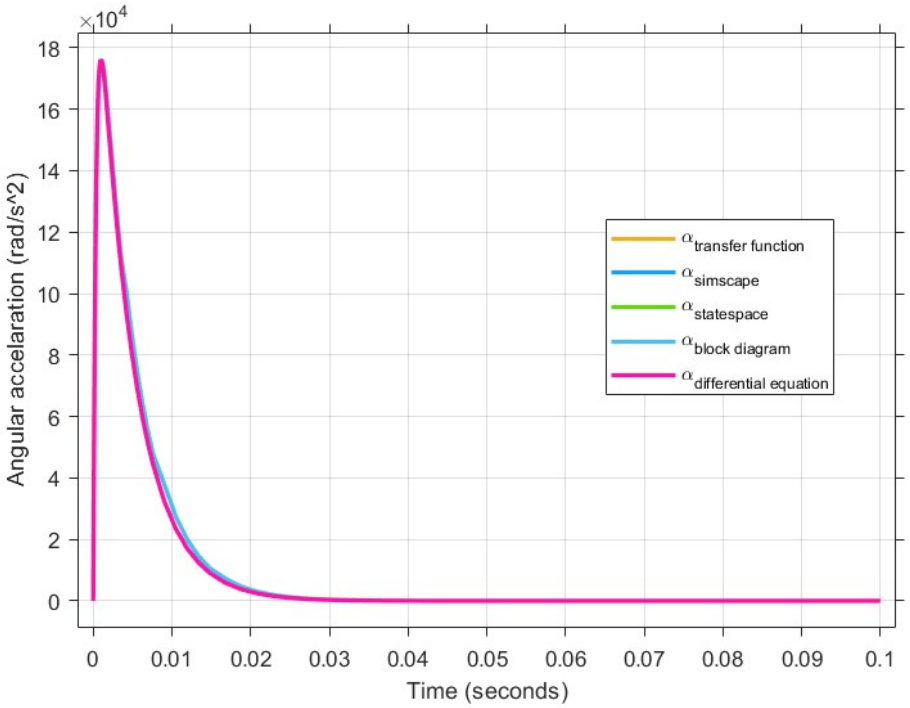

Figure 9: Verification of the models: α_{max}

From Figure 9 it is possible to see that maximum rotational acceleration in all the models is equal to $\dot{\omega}_{max} = 170 * 10^3\ rad/s^2$, which is a value with an acceptable error compared to the data sheet value shown above.

2.3 Angular velocity ω

Angular velocity is compared to no-load speed:

$$\omega_0 = 9700\ rpm$$

Mechanical time constant is also verified (time at which the mechanical property is at 63% of the steady value):

$$\tau_m = 4.9\ ms$$

All the conceptual models match up with each other, therefore only one plot is presented for all the aforementioned models is presented.

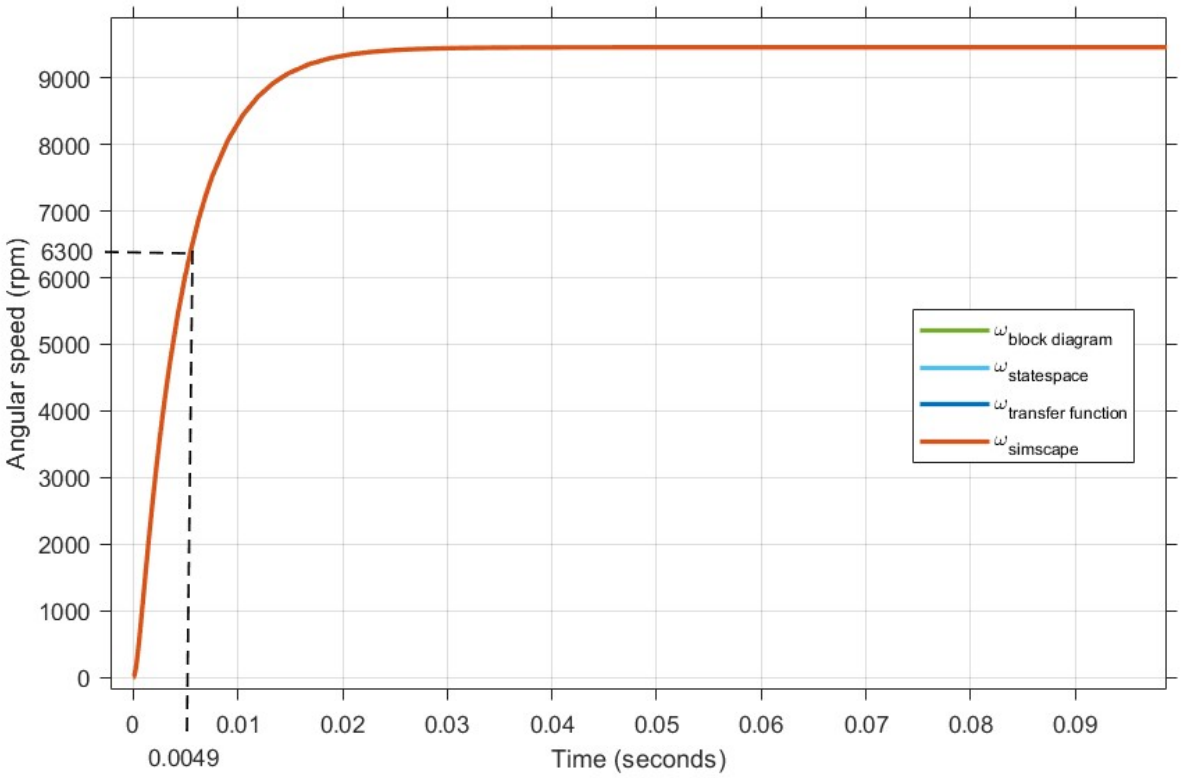

Figure 10: Verification of the models: τ_m and ω_0.

Figure 10 shows that steady-state velocity of the model matches up exactly with the data sheet value, as well as the value for the mechanical time constant.

It is possible to claim that the produced conceptual models represent the reality of the motor well and therefore are a good base subsystem to further construct the whole nut runner system.

3 Task 3

This section presents the controller parameters and system response for a step reference of 12 $\frac{\text{rad}}{\text{s}}$, as specified in Task 3. In this task, the angular velocity of the rotor is assumed to be measured by a sensor, which provides feedback to the controller. As shown in Figure 11, the current never exceeds the allowable limit of 500% of the rated current, with a peak of 7 amperes. The voltage peaks at 5.7 volts, and the system achieves 0% overshoot. The control parameters for the PI controller are $P = 0.22$ and $I = 6.46$.

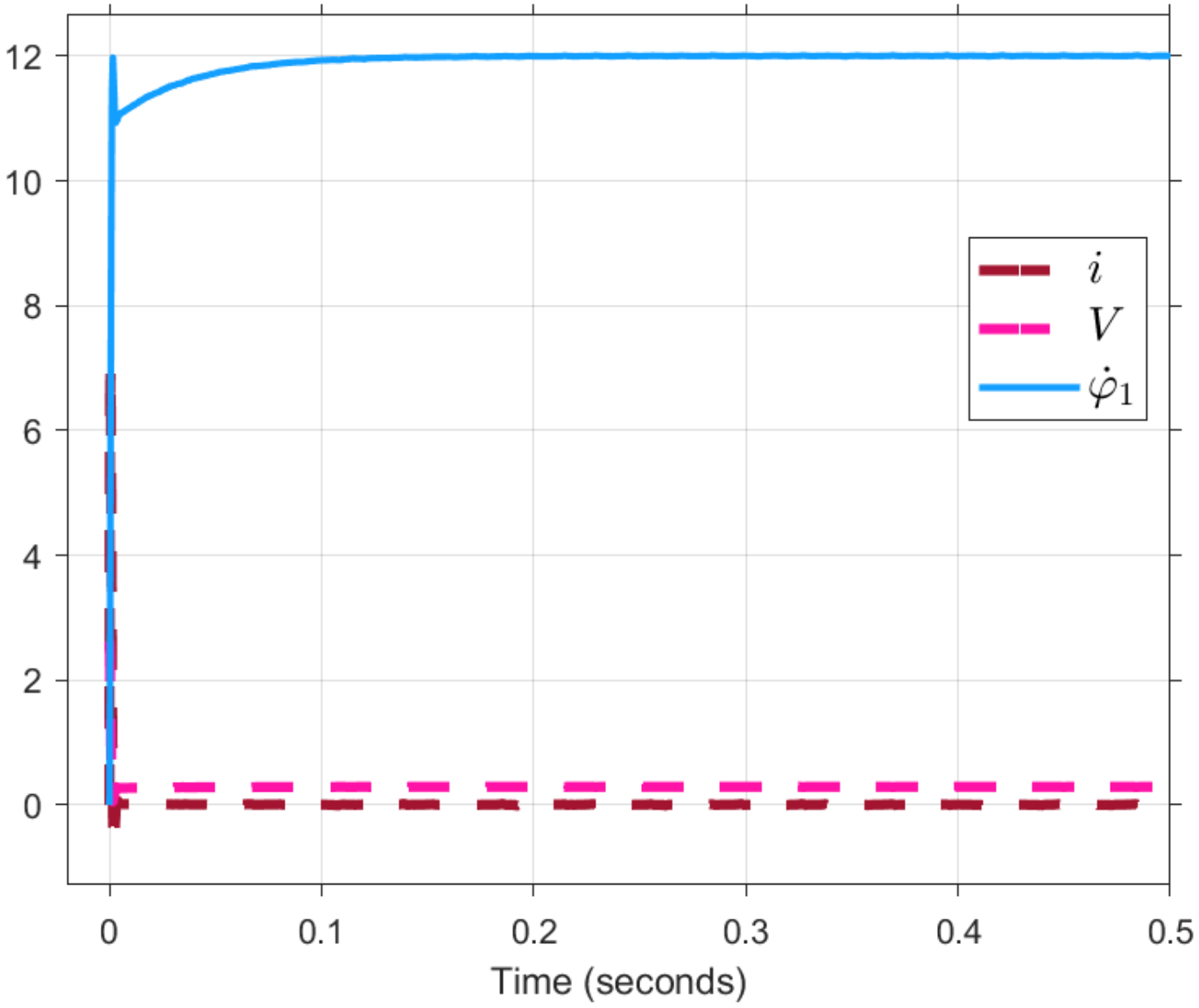

Figure 11: System response showing: current i, input voltage V, and DC motor angular velocity $\dot{\varphi}_1$.

4 Task 4

4.1 Pole Analysis and Model Simplification

The analysis begins with the transfer function(Equation (11)) derived in Section 1.4, leading to the characteristic equation of the model as Equation (12).

$$(Js + frT)(Ls + R) + K_m K_e = 0 \tag{12}$$

By expanding it, we obtain Equation (13).

$$JLs^2 + (JR + Lf_{rT})s + (Rf_{rT} + K_m K_e) = 0 \tag{13}$$

Equation (13) can be solved for the poles in Matlab with the command `P = pole(sys_tf)`. As a result, the poles are as Equation (14).

$$p_1 = -0.2212 \times 10^3, \quad p_2 = -2.7931 \times 10^3 \tag{14}$$

Among these, pole p_1 is significantly closer to the origin on the s-plane compared to p_2, indicating a slower response and a larger time constant. This observation allows us to consider p_1 as the dominant pole in the system, permitting the neglection of pole p_2. Given the relatively minor effect of the inductance $L = 73\,\mu H$ on system's dynamics, it can be omitted for simplification purposes. The characteristic equation (Equation (13))) can be simplified to first order as Equation (15) and (16).

$$\cancel{JLs^2} + (JR + \cancel{Lf_{rT}})s + (Rf_{rT} + K_m K_e) = 0 \tag{15}$$

$$JRs + (Rf_{rT} + K_m K_e) = 0 \tag{16}$$

4.2 Differential equations

With the omission of L, the original differential equations(Equation (1) and (2))) derived in Section 1.1 can be simplified as Equation (17) and (18).

$$V(t) = Ri(t) + K_e\omega(t) \tag{17}$$

$$J\frac{d\omega(t)}{dt} = K_m i(t) - frT\omega(t) \tag{18}$$

4.3 Block diagram (Simulink)

According to the differential equations derived in Section 4.2, we graphically represent the model with block diagram in Simulink as shown in Figure 12.

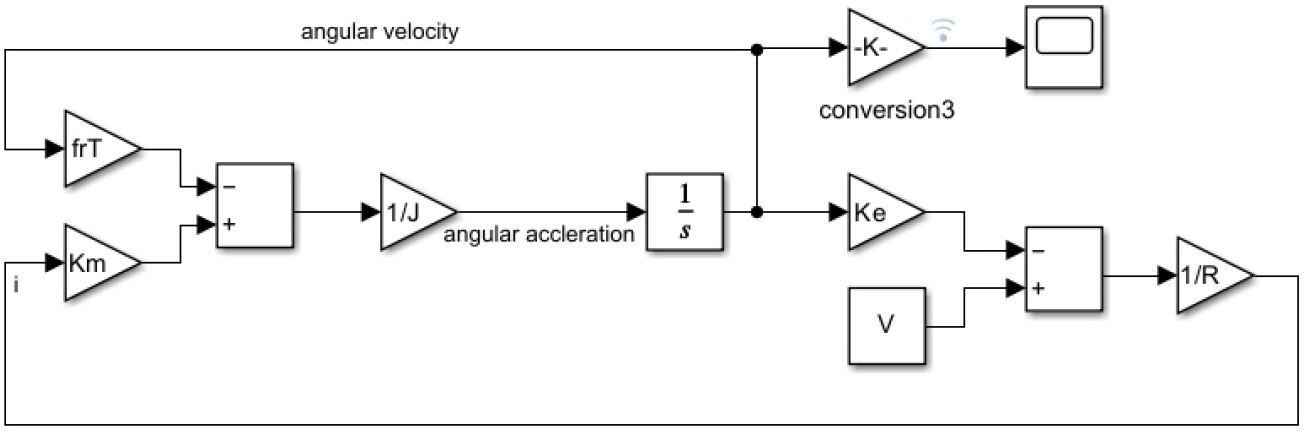

Figure 12: Block diagram of the simplified model

4.4 Transfer function model (Symbolically in MATLAB + Simulink)

With the simplified characteristic equation(Equation (16)), the simplified transfer function can be written as Equation (19).

$$\frac{\Omega(s)}{V(s)} = \frac{K_m}{JRs + K_m K_e + RfrT} \tag{19}$$

With Equation (19), we symbolically represent the simplified model in Matlab as Figure 13. To obtain the model in Simulink, we utilize the transfer function block as in shown Figure 14.

```
num2 = Km;
den2 = [J*R (Km*Ke+R*frT)];

sys_tf2 = tf(num2,den2);
```

Figure 13: Simplified transfer function model in Matlab

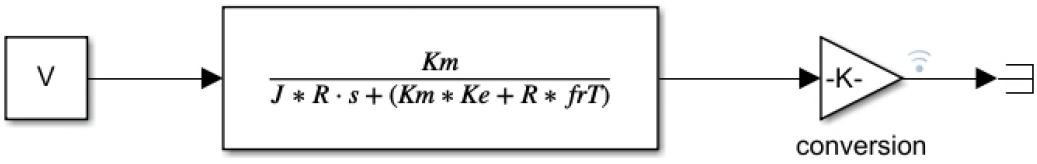

Figure 14: Simplified transfer function model in Simulink

4.5 Multidomain physical model (Simscape)

In the Simscape model, where the inductance is removed as in Figure 15.

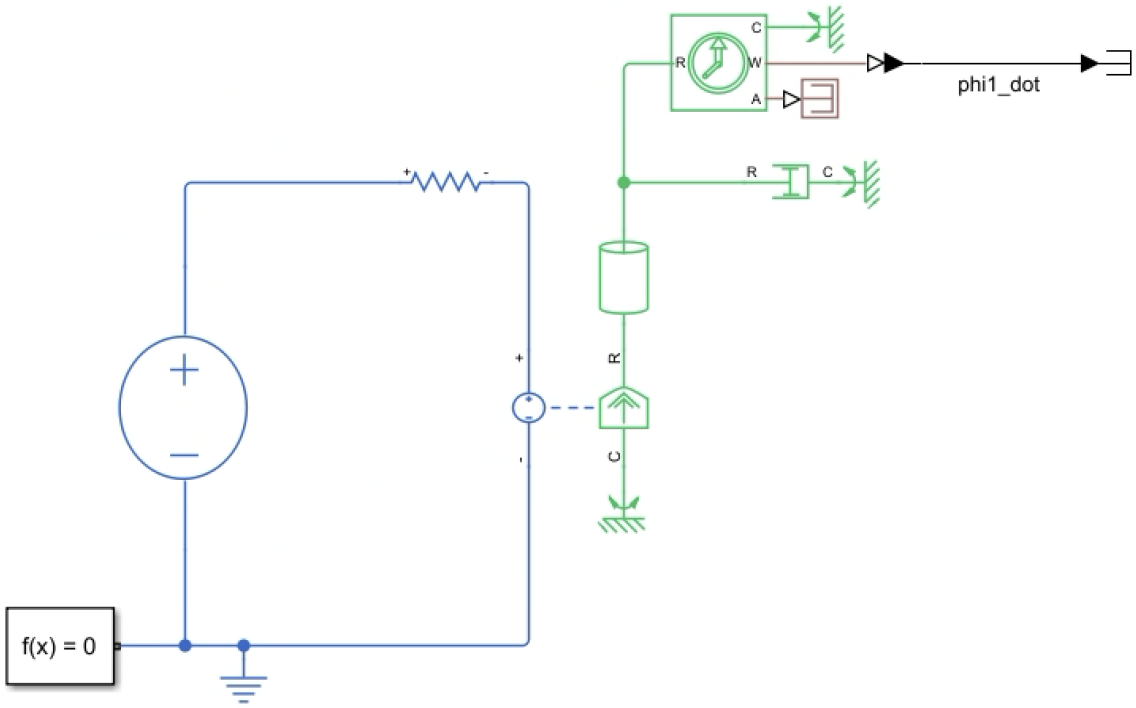

Figure 15: Simplified multidomain physical model in Simscape

4.6 Results of the Models

The simplified models are verified by comparing how they responded to the same input. The angular velocity outputs from the block diagram, transfer function, and Simscape models matched as shown in Figure 16.

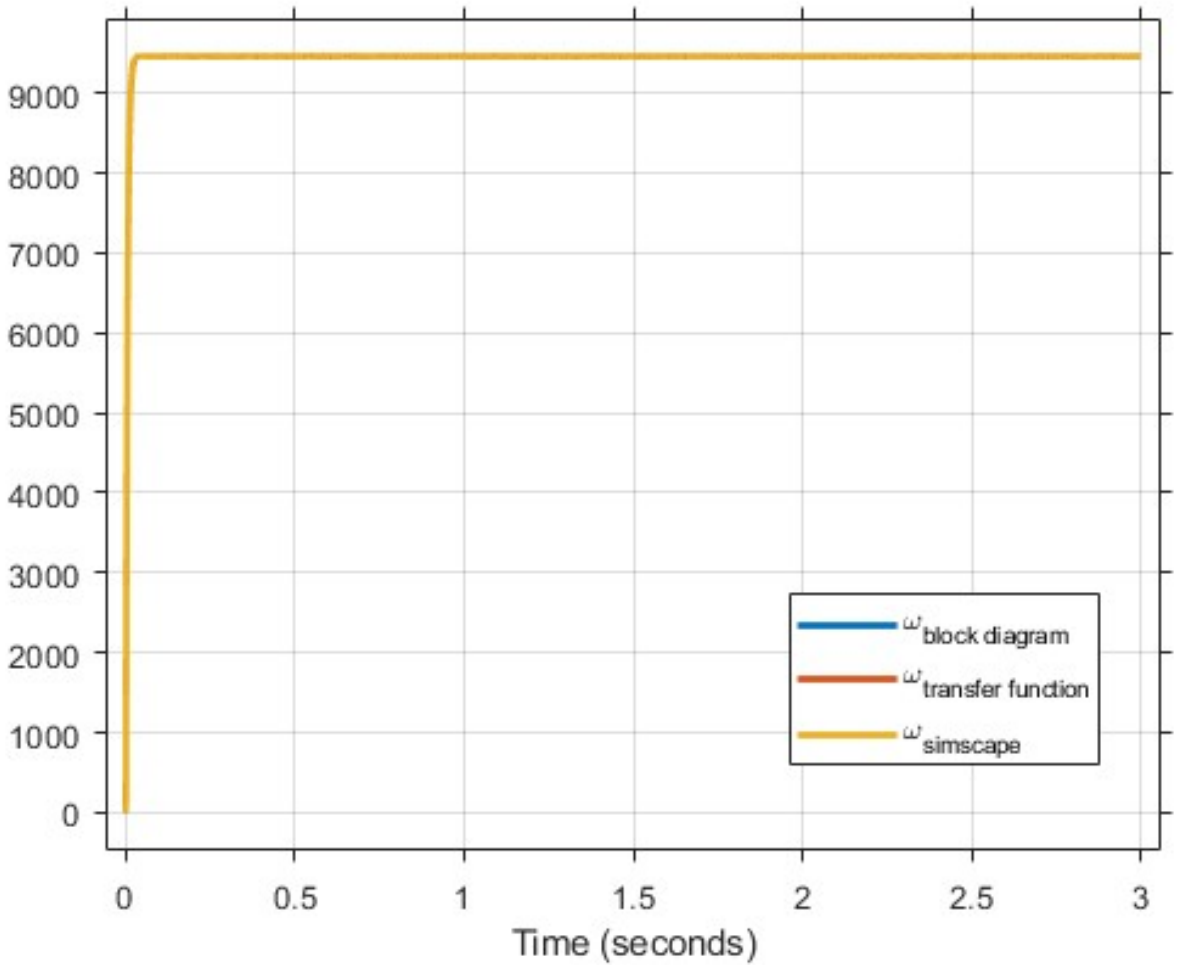

Figure 16: Results of ω based on different simplified models

5 Task 5

This section aims to determine the required gear ratio for the nut runner. The required maximum output torque of the nut runner is 55 Nm. To achieve this, the stall torque of the DC motor must be considered. Since the nut runner is not expected to run continuously and the lowest angular velocity of the output at peak output torque is not explicitly defined, it is possible to utilize the stall torque to determine the minimum total gear ratio, as per Equation (20):

$$n = \frac{55\,\text{Nm}}{\text{Stall Torque}} = 20.87286... \tag{20}$$

This total gear ratio ensures that the maximum output torque of the nut runner will be 55 Nm. The individual gear ratios for each planetary gear n_1, n_2 is calculated as per Equation (21).

$$n_1 = n_2 = \sqrt{n} = 4.568683... \tag{21}$$

However, the gear ratios n_1, n_2 is not feasible in practice, as the division of gear teeth limits the selection to rounded values. In a real-world application, the gear ratio would need to be rounded up to an available gear ratio to ensure the required torque output of 55 Nm.
Also, some extra margin would be beneficial to ensure that the nut runner can achieve the 55 Nm at a satisfactory angular velocity, with the current gear ratio the velocity will be at zero. Since the lowest angular velocity at peak output torque is not explicitly defined in the assignment, and the objective is to model the dynamics of the nut runner, the theoretically smallest gear ratio is used and kept for the calculations of the following tasks.

6 Task 6

In this section, the dynamic behaviour of the nut runner system during the run-down phase is modelled. The derived equations and state-space representation, outlined in Section 6.1, describe the system's inertia, torques, and angular acceleration. The model is then verified through simulation and analysis in Section 6.2, forming the basis for further tasks.

6.1 Models and Equations

This section presents an analysis of the dynamic system representing the mechanical and electrical components of the nut runner system during the run-down phase. The following equations,along with the free body diagram, Figure 17, describe the system's inertia, torques, and dynamic behaviour.

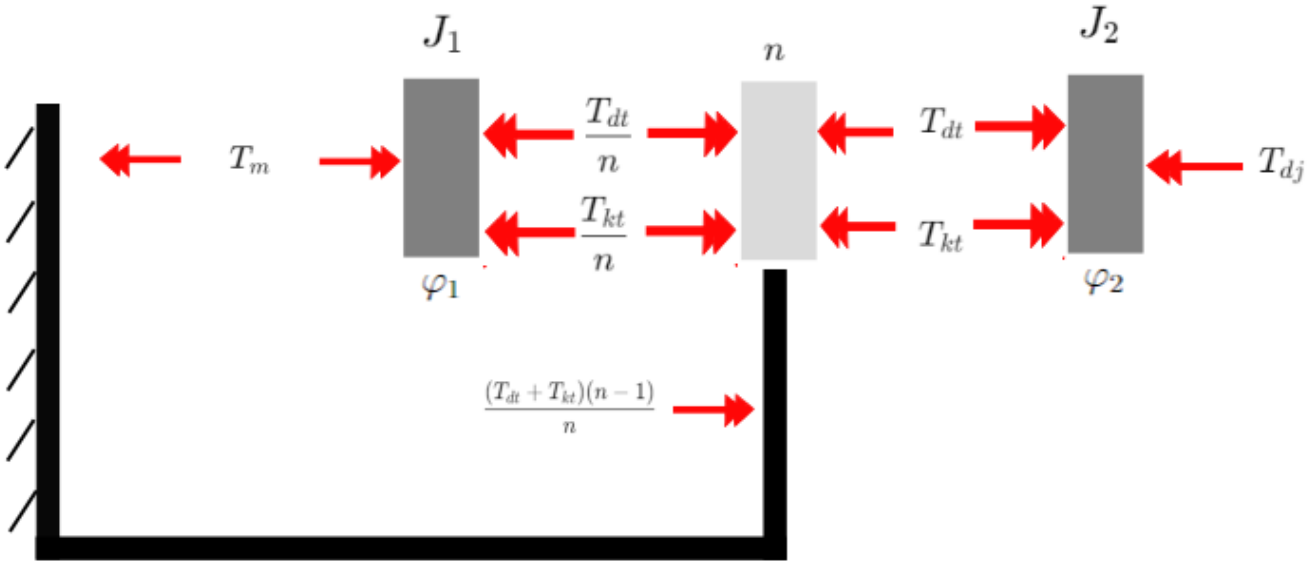

Figure 17: Free body diagram of the nut runner system during the run-down phase

The equivalent inertia for the rotor, input shaft, and gears on the input side of the gears is defined as J_1 by Equation (22).

$$J_1 = J_{\text{rotor}} + J_{g1} + J_{\text{in\_shaft}} + \frac{J_{g2}}{n_1^2} \tag{22}$$

Where J_{rotor} is the rotor inertia, J_{g1} is the inertia of the first gear, $\frac{J_{g2}}{n_1^2}$ is the inertia of the second gear, divided by the square of the gear ratio n_1, and $J_{\text{in\_shaft}}$ is the estimated inertia for the input shaft, calculated using an estimated steel density of 7850 kg/m^3 and provided drawings.
The inertia J_2 for the output shaft is calculated the same way as for the input shaft $J_{\text{in\_shaft}}$ calculated from the drawings and with an estimated steel density of 7850 kg/m^3, as shown in Equation (23).

$$J_2 = \frac{1}{2} V_{\text{out\_axle}} \cdot \rho \cdot \left(\overline{r_1}^2 + \overline{r_2}^2\right) \tag{23}$$

Where ρ is the density of steel, $V_{\text{out\_axle}}$ represents the volume of the output shaft, and $\overline{r_1}, \overline{r_2}$ is the average inner and outer radius of the shaft over its length. Equation (22) and (23) gives the iniertias $J_1 = 13.567 \times 10^{-6}$ and $J_2 = 2.426 \times 10^{-6}$.

The torque generated by the motor, T_m, is given by Equation (24). It depends on the motor constant K_m, resistance R, input voltage V, back-EMF constant K_e, and friction frT.

$$T_m = \frac{K_m}{R}\left(V - K_e\dot{\varphi}_1\right) - \mathrm{frT}\dot{\varphi}_1 \tag{24}$$

The torque T_{dj} caused by the damping characteristics of the screw is defined by Equation (25).

$$T_{\mathrm{dj}} = d_j\dot{\varphi}_2 \tag{25}$$

The torque T_{dt} caused by the damping characteristics of the gears is defined by Equation (26).

$$T_{\mathrm{dt}} = d_t\left(\frac{\dot{\varphi}_1}{n} - \dot{\varphi}_2\right) \tag{26}$$

The torque T_{Kt} caused by the spring characteristics of the gears is defined by Equation (27).

$$T_{\mathrm{Kt}} = K_t\left(\frac{\varphi_1}{n} - \varphi_2\right) \tag{27}$$

The angular acceleration for the input rotational bodies, derived from the free body diagram (Figure 17), is given by Equation (28).

$$\ddot{\varphi}_1 = \frac{1}{J_1}\left(T_m - \frac{T_{\mathrm{Kt}}}{n} - \frac{T_{\mathrm{dt}}}{n}\right) \tag{28}$$

Inserting Equations (24), (26), and (27) into Equation (28) gives the complete differential equation (29) for the angular acceleration of the input side of the gears.

$$\ddot{\varphi}_1 = \frac{1}{J_1}\left(\frac{K_m V}{R} - \frac{K_t}{n^2}\varphi_1 + \frac{K_t}{n}\varphi_2 - \left(\frac{d_t}{n^2} + \frac{K_m K_e}{R} + \mathrm{frT}\right)\dot{\varphi}_1 + \frac{d_t}{n}\dot{\varphi}_2\right) \tag{29}$$

The angular acceleration for the output rotational bodies is described by Equation (30).

$$\ddot{\varphi}_2 = \frac{1}{J_2}\left(T_{\mathrm{Kt}} + T_{\mathrm{dt}} - T_{\mathrm{dj}}\right) \tag{30}$$

Inserting Equations (25), (26), and (27) into Equation (30) gives the complete differential equation (31) for the angular acceleration of the output side of the gears, the load side.

$$\ddot{\varphi}_2 = \frac{1}{J_2}\left(K_t\frac{\varphi_1}{n} - K_t\varphi_2 + \frac{d_t}{n}\dot{\varphi}_1 - (d_j + d_t)\dot{\varphi}_2\right) \tag{31}$$

By translating Equations (29) and (31) to state-space form, Equation (32) and (34), the system dynamics are described by the matrices A, B, C, and D.

$$\dot{X} = AX + Bu \tag{32}$$

Where X defines the states in the state space model, defined as per Equation (33)

$$X = \begin{bmatrix} \varphi_1 \\ \varphi_2 \\ \dot{\varphi}_1 \\ \dot{\varphi}_2 \end{bmatrix} \tag{33}$$

$$Y = CX + Du \tag{34}$$

$$A = \begin{bmatrix} 0 & 0 & 1 & 0 \\ 0 & 0 & 0 & 1 \\ -\frac{K_t}{J_1 n^2} & \frac{K_t}{nJ_1} & -\frac{\left(\frac{d_t}{n^2} + \mathrm{frT} + \frac{K_m K_e}{R}\right)}{J_1} & \frac{d_t}{J_1 n} \\ \frac{K_t}{J_2 n} & -\frac{K_t}{J_2} & \frac{d_t}{nJ_2} & -\frac{d_j + d_t}{J_2} \end{bmatrix} \tag{35}$$

$$B = \begin{bmatrix} 0 \\ 0 \\ \frac{K_m}{RJ_1} \\ 0 \end{bmatrix} \tag{36}$$

$$C = \begin{bmatrix} 1 & 0 & 0 & 0 \\ 0 & 1 & 0 & 0 \\ 0 & 0 & 1 & 0 \\ 0 & 0 & 0 & 1 \end{bmatrix} \tag{37}$$

$$D = \begin{bmatrix} 0 \\ 0 \\ 0 \\ 0 \end{bmatrix} \tag{38}$$

Here, u represents the input, which in this case is the voltage applied to the motor. Since the matrix C in Equation (37) is a 4x4 identity matrix, the output Y includes all the system states. Y consists of the motor angle φ_1, motor angular velocity $\dot{\varphi}_1$, load angle φ_2, and load angular velocity $\dot{\varphi}_2$.
The D matrix, as seen in Equation (38), is a zero vector, which implies that the output Y is not directly dependent on the input u as seen in Equation (34). With C being a 4x4 identity matrix and D zero, Equation (34) can be simplified to Equation (39).

$$Y = X^T \tag{39}$$

6.2 Model Verification

To verify the state-space model derived in Section 6.1, the mechanical time constant and the correlation between the four states are examined and evaluated. This evaluation is performed by plotting the four states with a one-volt step input, as shown in Figures 18 and 19.

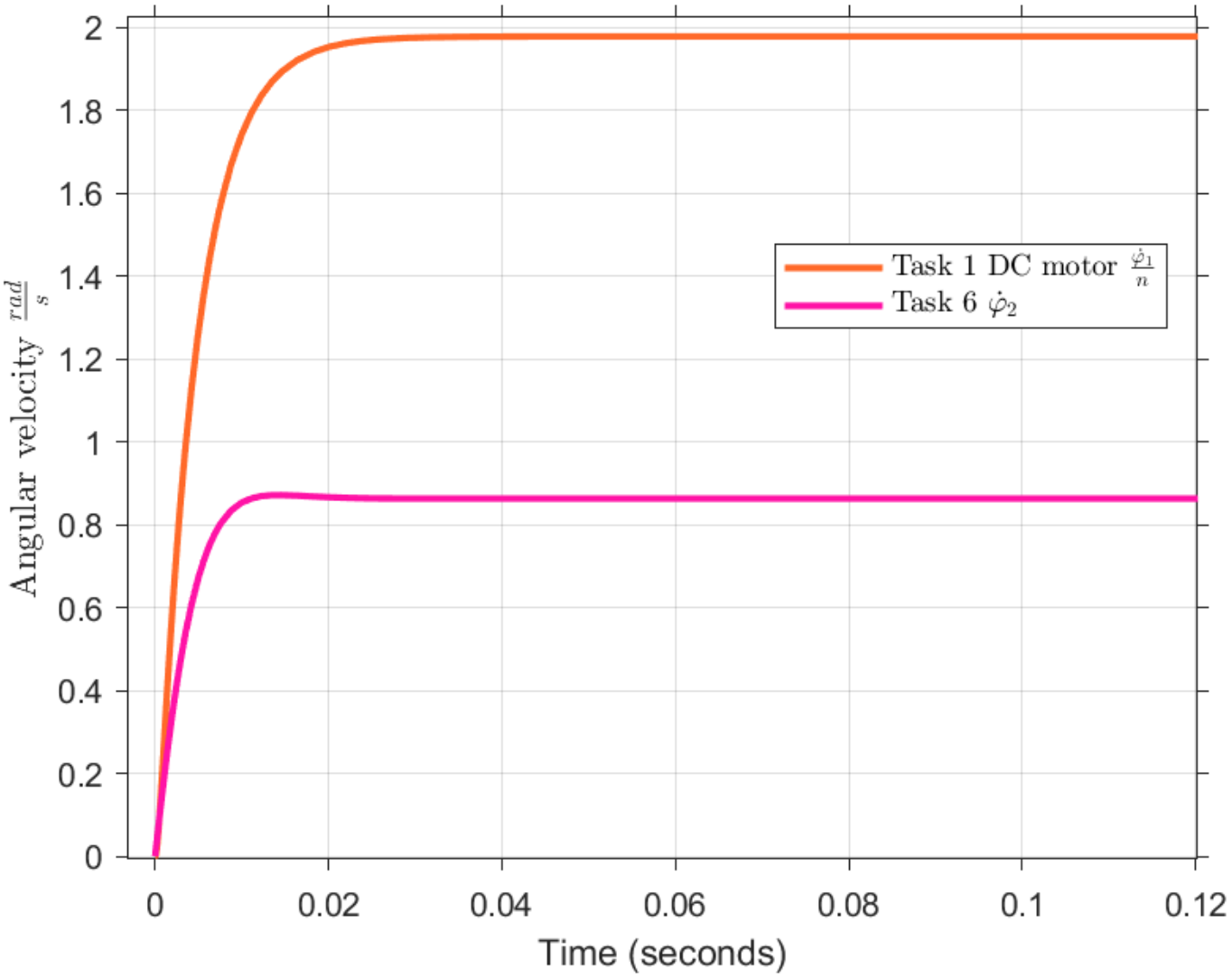

Figure 18: $\dot{\varphi}_2$ from the state-space model is compared to $\frac{\dot{\varphi}_1}{n}$ from Task 1, when the input u is a unit step.

In Figure 18, only the initial response to the 1 V step input is visualized. From the plot, it is possible to determine that the time constant for the entire system represented by the state space model is 0.004 seconds, and the saturated angular velocity of the output is 0.86 $\frac{\text{rad}}{\text{s}}$. The equivalent DC motor's mechanical time constant is 0.005 seconds, and its saturated velocity is 1.98 $\frac{\text{rad}}{\text{s}}$ [**datasheet**].

The mechanical time constant for the DC motor is higher than that of the nut runner system. This difference is due to the increased damping of the system. While larger inertia tends to increase the time constant, the inertia of the components in the system is relatively small compared to the damping coefficients of the system. Therefore, a smaller mechanical time constant is expected and is a reasonable result.

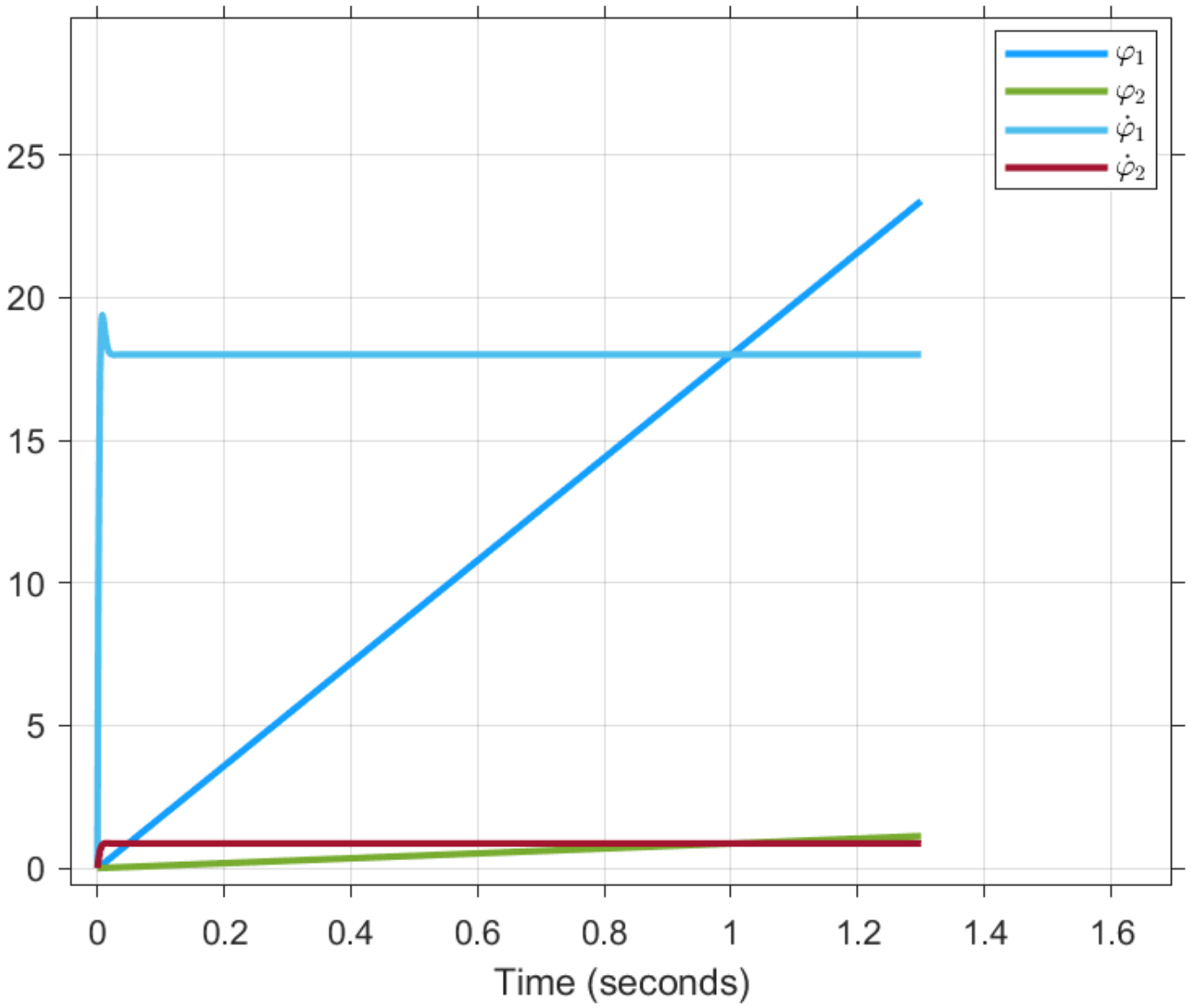

Figure 19: Y when u is a unit step.

In Figure 19, all of the system's states are visualized when the input u is a unit step. From the plot, it is possible to determine that the saturated angular velocity of the DC motor, $\dot{\varphi}_1$, is approximately 18 $\frac{\text{rad}}{\text{s}}$, while the output velocity, $\dot{\varphi}_2$, is approximately 0.9 $\frac{\text{rad}}{\text{s}}$. The two velocities are proportional by a factor of approximately n as expected since the output velocity is inversely related to the input velocity in a gear system. This is also true for the angle after the initial acceleration has been passed.

It is also notable that φ_1 intersects $\dot{\varphi}_1$ at approximately one second, and similarly, φ_2 intersects $\dot{\varphi}_2$ at the same time. This behaviour is expected since the initial acceleration to the saturated velocity occurs over less than 0.023 seconds. Hence, the average velocity during the first second is close to the saturated velocity, the angle should intersect the angular velocity at one second. To conclude the model verification, the results match the expected behaviour of the system, and therefore the following tasks can rely on the model derived in Section 6.1.

7 Task 7

This section presents the controller parameters and system response for the reference velocity specified in Task 7. For this task, it is assumed that the velocity sensor is placed on the motor side of the gears, as this would be the most realistic scenario. With the controller parameters $P = 1.2$ and $I = 51$, the output speed closely follows the reference velocity, while maintaining the voltage within the allowable range of $0 - 24$ V. If reverse polarity were allowed, the controller parameters could be increased, resulting in improvements in response time and smaller steady-state errors. As shown in Figure 20, the controller follows the reference velocity, achieving a steady-state error of approximately 2.3% on the ramps and 0% on the flat section.

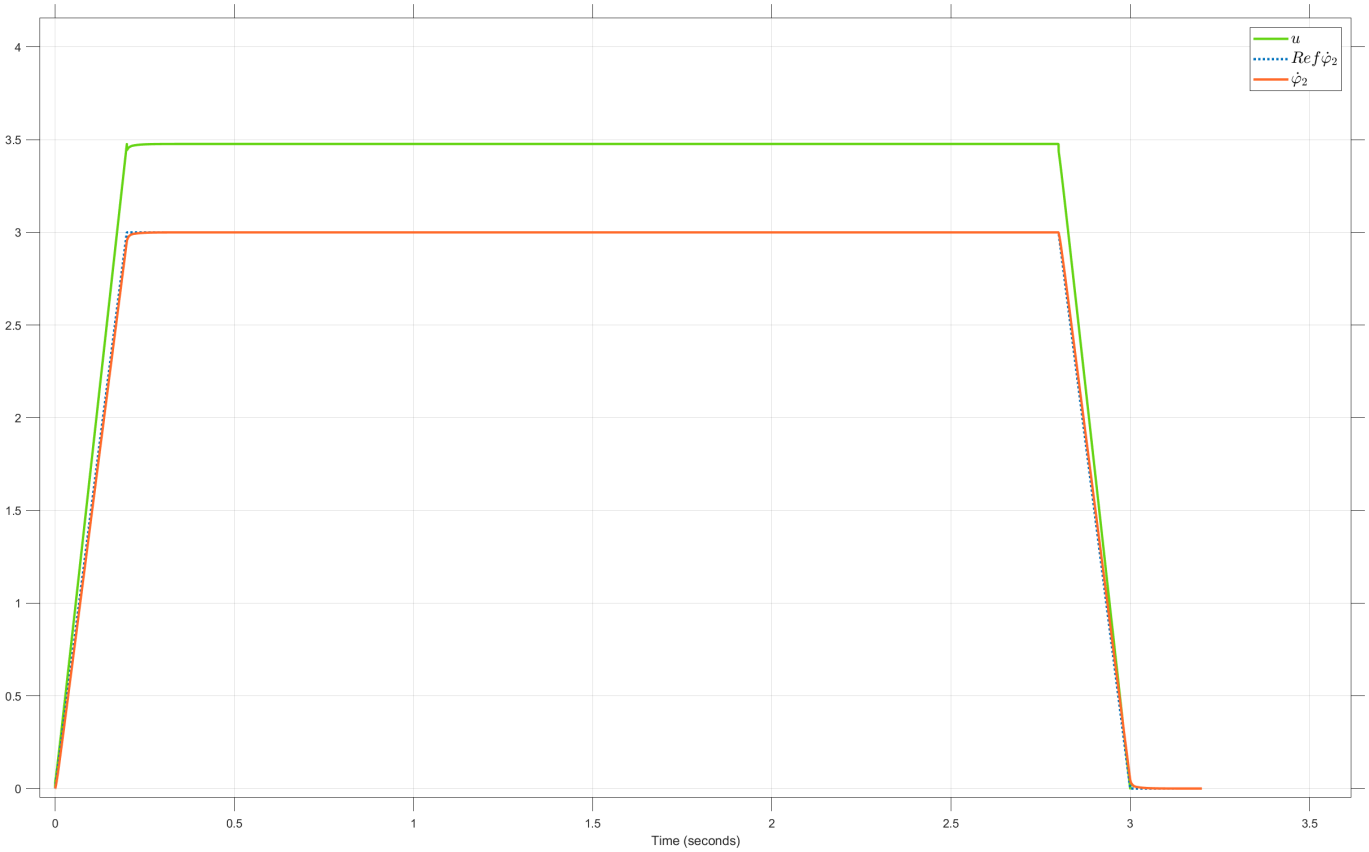

Figure 20: System response showing reference velocity Ref $\dot{\varphi}_2$, actual system response $\dot{\varphi}_2$, and input voltage u.

8 Task 8

This task deals with the modelling of the resistance to tightening of the screw. The screw is M8 and of strength class 8.8 ($\sigma_{fract} = 800\ MPa$, $\sigma_{yield} = 640\ MPa$), pitch $p = 1.25\ mm$, and free length $L_0 = 100\ mm$.
Here only the elastic clamping phase of the tightening is modelled, and the screw resistance is modelled as a rotational spring of spring constant value k_j.

8.1 Rotational spring constant k_j

The value for k_j is calculated using an energy approach: the translational elastic energy stored while the screw deforms under tightening is set equal to the torsional elastic energy stored.

$$\frac{1}{2}k_s\Delta x^2 = \frac{1}{2}k_j\Delta\varphi_2^2 \tag{40}$$

Where k_s is the theoretical translational screw spring constant if the screw is assumed to be a beam-element, Δx is the deformation of the screw and $\Delta\varphi_2$ is the angle of rotation of the screw after the clamping phase has started.
Knowing that the relationship between Δx and $\Delta\varphi_2$ is regulated by the pitch p, meaning that the ratio $\frac{\Delta x}{\Delta\varphi_2} = \frac{p}{2\pi}$ is constant, and that k_s can be defined with basic beam-theory by $k_s = \frac{EA}{L}$, where $E = 200\ GPa$ is materials Young's modulus, A is screw cross-sectional area and L is total length of the screw, it can be derived that:

$$k_j = \frac{EA}{L}\ (\frac{p}{2\ \pi})^2 = 4\ Nm/rad^2 \tag{41}$$

8.2 State space model updated

The state space model is now updated so that it can take into account the newly calculated factor k_j. The only change that happens in the model is located in the A matrix (position A_{42}):

$$\dot{X} = AX + Bu \tag{42}$$

Where X is

$$X = \begin{bmatrix} \varphi_1 \\ \varphi_2 \\ \dot{\varphi}_1 \\ \dot{\varphi}_2 \end{bmatrix} \tag{43}$$

$$Y = CX + Du \tag{44}$$

$$A' = \begin{bmatrix} 0 & 0 & 1 & 0 \\ 0 & 0 & 0 & 1 \\ -\frac{K_t}{J_1 n^2} & \frac{K_t}{nJ_1} & -\frac{\left(\frac{d_t}{n^2}+\mathrm{frT}+\frac{K_m K_e}{R}\right)}{J_1} & \frac{d_t}{J_1 n} \\ \frac{K_t}{J_2 n} & -\frac{K_t+K_j}{J_2} & \frac{d_t}{nJ_2} & -\frac{d_j+d_t}{J_2} \end{bmatrix} \tag{45}$$

$$B = \begin{bmatrix} 0 \\ 0 \\ \frac{K_m}{RJ_1} \\ 0 \end{bmatrix} \tag{46}$$

$$C = \begin{bmatrix} 1 & 0 & 0 & 0 \\ 0 & 1 & 0 & 0 \\ 0 & 0 & 1 & 0 \\ 0 & 0 & 0 & 1 \end{bmatrix} \tag{47}$$

$$D = \begin{bmatrix} 0 \\ 0 \\ 0 \\ 0 \end{bmatrix} \tag{48}$$

Where φ_1 and φ_2 are motor/transmission angles (1: motor side, 2: tool side of angle gear).

8.3 Torque evaluation and corresponding turning angle

The torque on the nut for a voltage input of $V = 24V$ can be calculated through the Simulink block shown in Figure 21:

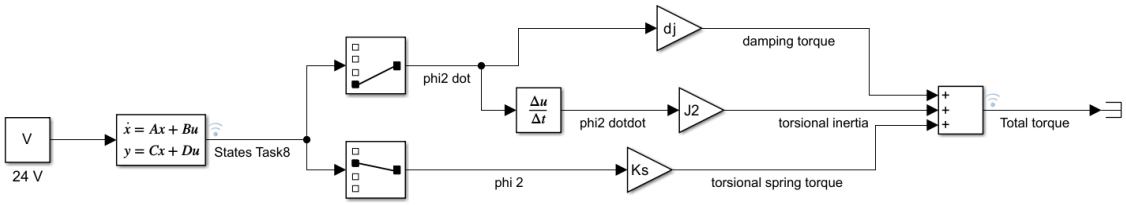

Figure 21: Simulink block to calculate total torque

The steady-state total torque is found to be:

$$T_{tot} = 55Nm$$

The corresponding turning angle in the clamping phase can be calculated with Equation 49.

$$\Delta\varphi_2 = \frac{T_{tot}}{k_j} \tag{49}$$

Therefore the total turning angle of the clamping phase is:

$$\Delta\varphi_2 = 13.75\ rad = 2.18\ rotations$$

9 Task 9

This section presents the controller parameters and system response for the reference velocity specified in Task 9, where the reference is 3 $\frac{\text{rad}}{\text{s}}$ until the output reaches 25 Nm. For this task, it is assumed that the velocity sensor is placed on the motor side of the gears, which is a realistic scenario. Hence, the reference velocity has been scaled by the gear ratio n. First, a P controller is presented in Section 9.1, followed by a PI controller in Section 9.2.

9.1 P Controller

With the controller parameter P defined as in Equation (50), the initial input to the system remains within the allowed 24 volts. However, due to the torque acting as a disturbance, the P controller does not achieve the target angular velocity of 3 $\frac{\text{rad}}{\text{s}}$ at the output. As shown in Figure 22, the angular velocity $\dot{\varphi}_2$ peaks at 2.6 $\frac{\text{rad}}{\text{s}}$.

$$P = \frac{24}{3n} \tag{50}$$

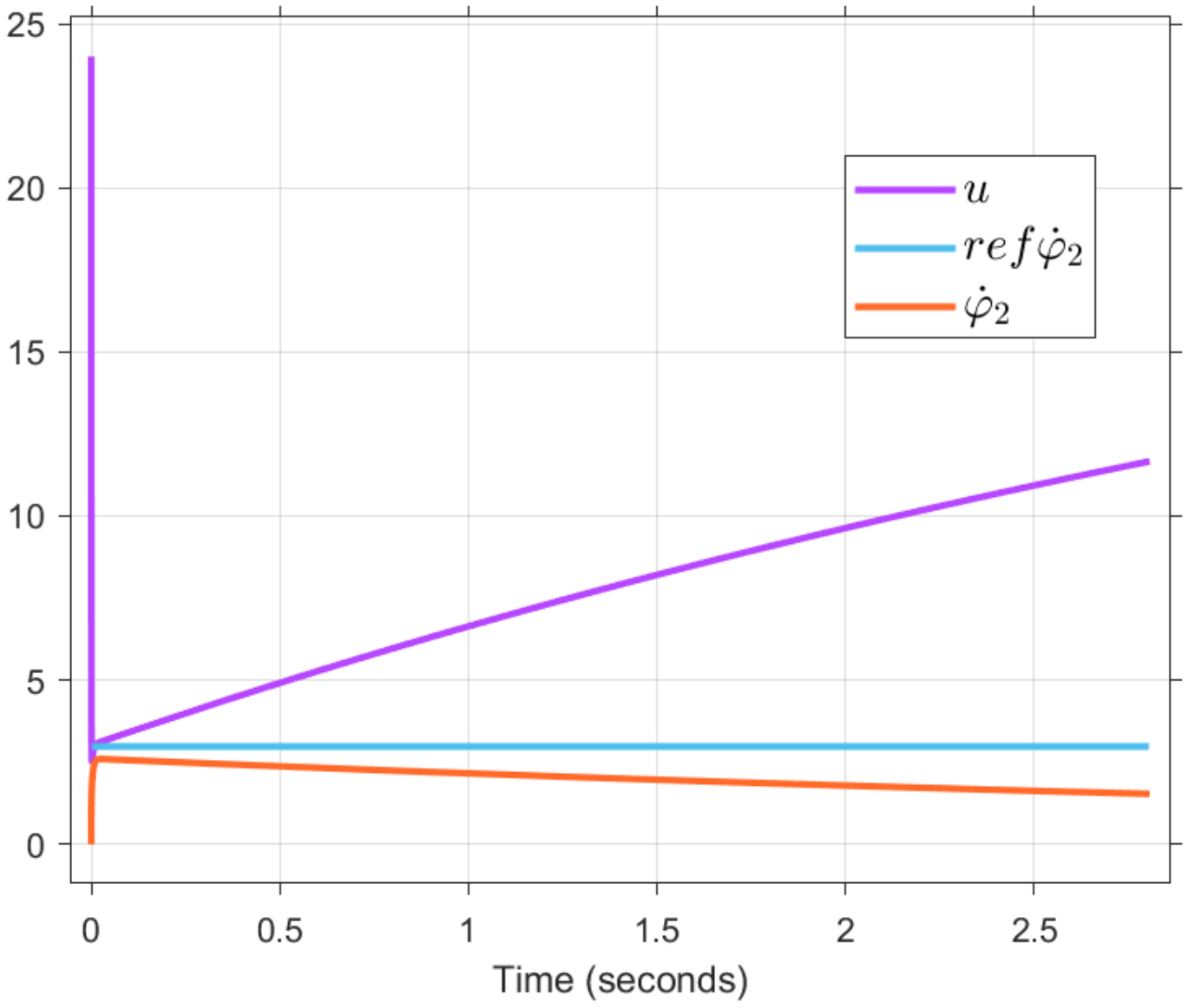

Figure 22: System response using the P controller, showing the angular velocity $\dot{\varphi}_2$, reference $ref\dot{\varphi}_2$, and input voltage u.

9.2 PI Controller

Introducing an integral term to the P controller creates a PI controller, which should mitigate the steady-state error. However, there is a limitation: if the integral gain I is too large, the system starts to oscillate. The proportional gain P is kept the same as in the P controller in Section 9.1, and the integral constant is set to $I = 1200$. This value is at the limit of the controller, as a higher I would cause the output voltage to go negative. Even with this configuration, a 0,53% steady-state error remains, as shown in Figure 23.

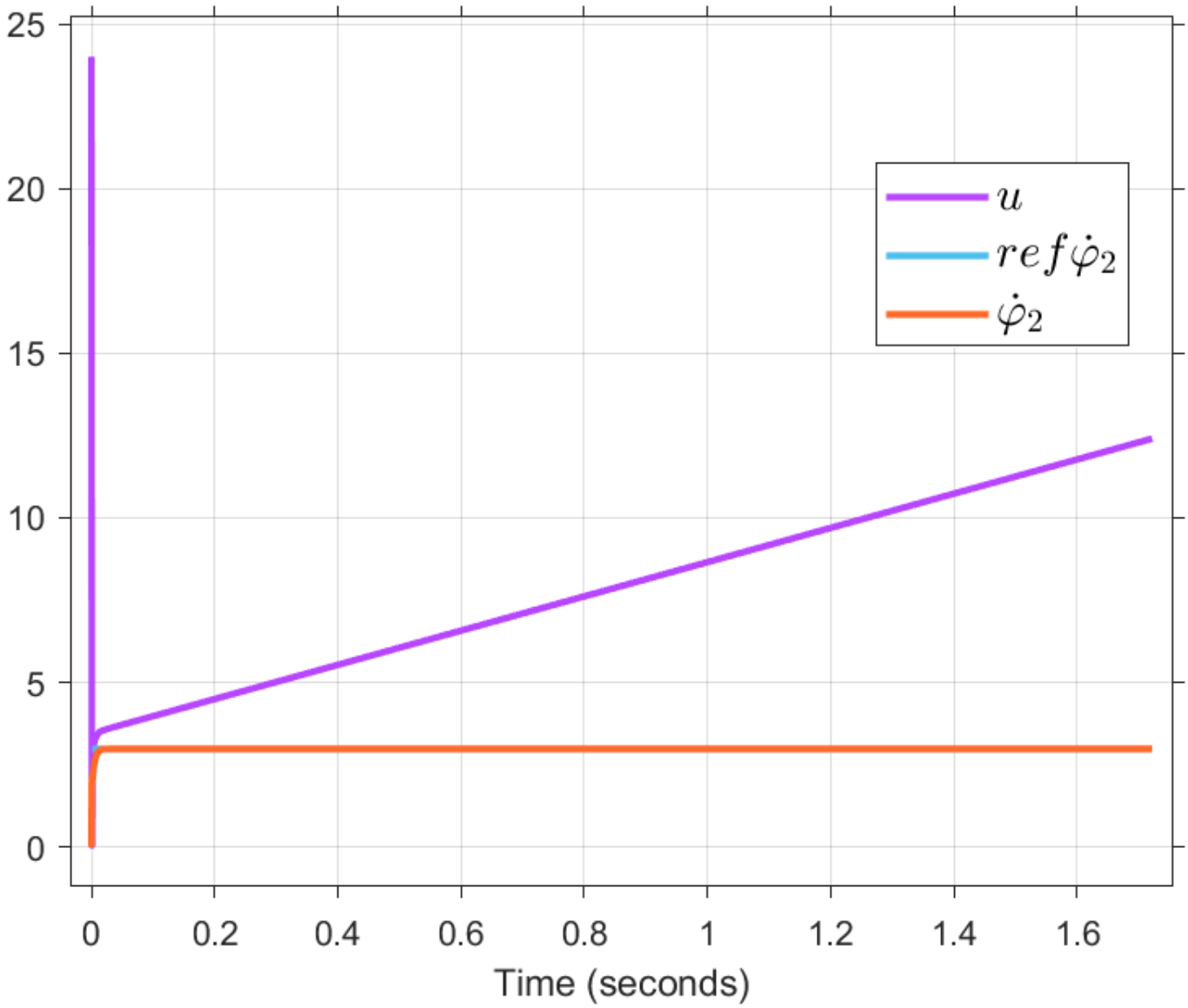

Figure 23: System response using the PI controller, showing the angular velocity $\dot{\varphi}_2$, reference $ref\dot{\varphi}_2$, and input voltage u

A pre-filter was implemented to reduce the steady-state error further. A gain of $K_{\text{pf}}\frac{3}{2.984}$ was applied to the reference signal. To prevent voltage saturation from the PI controller, the proportional gain P was divided by the prefilter gain K_{pf}, and the integral gain I was kept. This resulted in the following constants: $P = 0,381$, $I = 1200$, and pre-filter gain $K_{\text{pf}} = 1,0067$. With this configuration, the system achieves 0% steady-state error while staying within the 0-24 volt range, as seen in Figure 24.

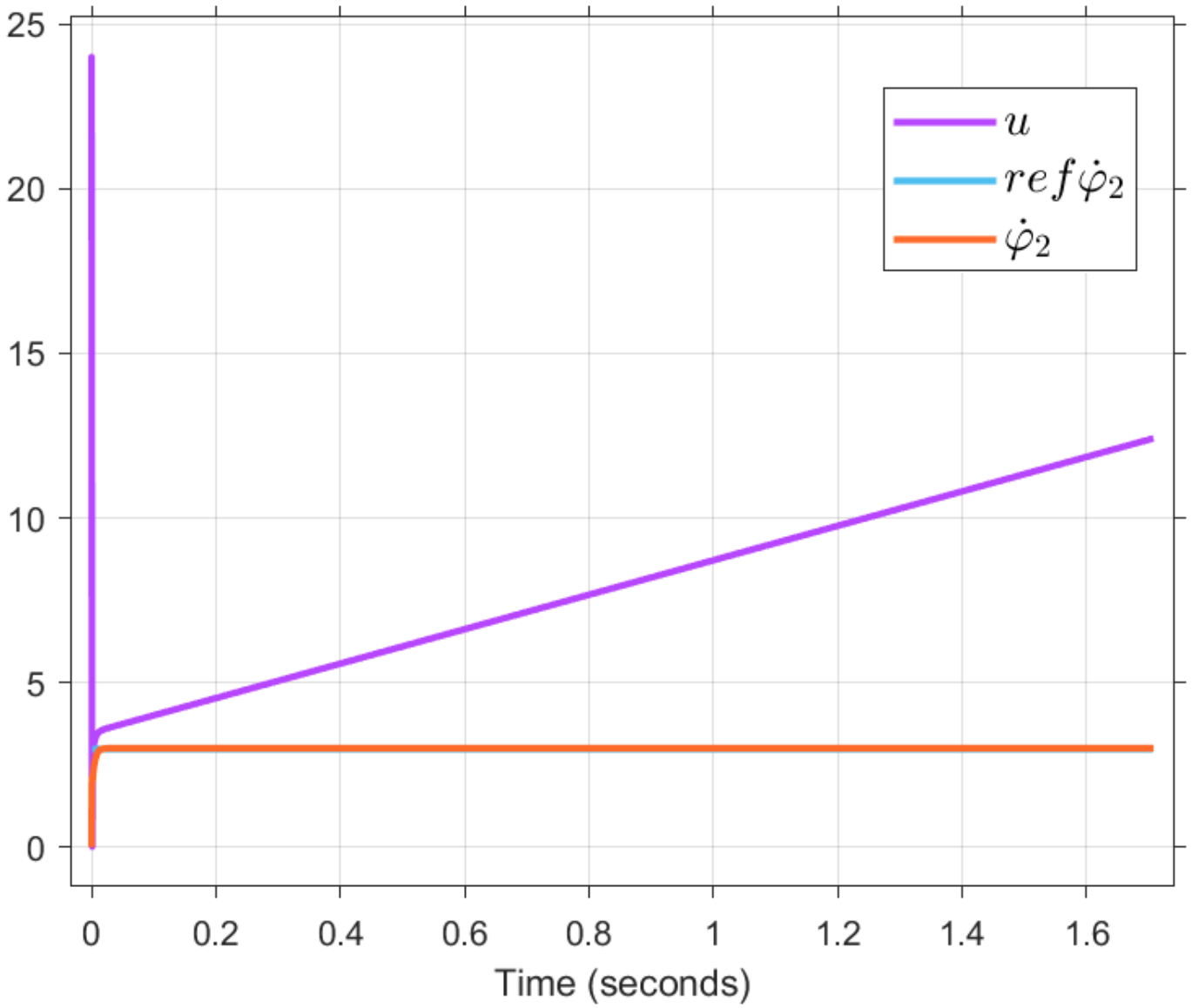

Figure 24: System response using the pre-filter PI controller, showing the angular velocity $\dot{\varphi}_2$, reference $ref\dot{\varphi}_2$, and input voltage u

10 Task 10

This section's aim is to evaluate if the tightening of the nut is in good order with respect to the strength properties of the screw, comparing the effective normal stress in the screw with the material's yield strength (here $\sigma_{yield} = 640\ MPa$).
A factor that takes into account Coulomb's friction is also introduced later, to better represent the physical behavior of the screw tightening process.
How large is the tightening nut angle?

10.1 Stress considerations

First, the stress in the screw is evaluated based on the aim torque of 25 Nm without considering friction through Simulink model simulation (Figure 25):

$$\sigma_{25Nm} = 2000\ MPa$$

with a tightening angle on the output side of:

$$\Delta\varphi 2_{25Nm} = 5.1\ rad$$

This stress is way above the yield stress of the screw, therefore some adjustments, such as the introduction of Coulomb's friction or reducing of aim torque have to be applied.
For example here an aim torque of just $T_{aim} = 11\ Nm$ would achieve yielding in the screw.

10.2 Coulomb's friction

The model is now extended to simulate Coulomb friction between nut and screw, thus introducing a torque opposing nut rotation following Equation 51:

$$T_{friction} = \mu F_s r_s \tag{51}$$

where μ is the friction coefficient, F_s the screw force and r_s the nominal radius of the thread. Typical friction coefficients can be in the range 0.1 – 0.2. Here a friction coefficient of $\mu = 0.1$ is assumed.
The stress found for a $T_{aim} = 25\ Nm$ is:

$$\sigma_{25Nm,0.1} = 680MPa$$

with a tightening angle on the output side of:

$$\Delta\varphi_{25Nm,0.1} = 1.7\ rad$$

This value of aim torque combined with the newly introduced friction coefficient still takes the screw to yielding, meaning that it still isn't ideal for this application.

10.3 Final parameters

An adjustment on the aim torque is made so that it is possible to reach a stress in the screw close to yielding strength.
The final aim torque for a friction value $\mu = 0.1$ is set to:

$$T_{aim} = 23.8\ MPa$$

which takes the stress in the screw close to yielding but below:

$$\sigma_{23.8,0.1} = 630\ MPa$$

It is found that the controller parameters don't need any adjustment with the new setup.

10.4 Deflection twist in the transmission

The twist in the transmission is found evaluating the difference between output rotations (φ_2) and motor rotations (φ_1) at the end of the process, respectively scaled with the gear ratio n.
Load side transmission twist:

$$\Delta\varphi_{out} = \frac{\varphi_1}{n} - \varphi_2 = 0.0147\ rad$$

Motor side transmission twist:

$$\Delta\varphi_{mot} = \varphi_1 - \varphi_2 * n = 0.308\ rad$$

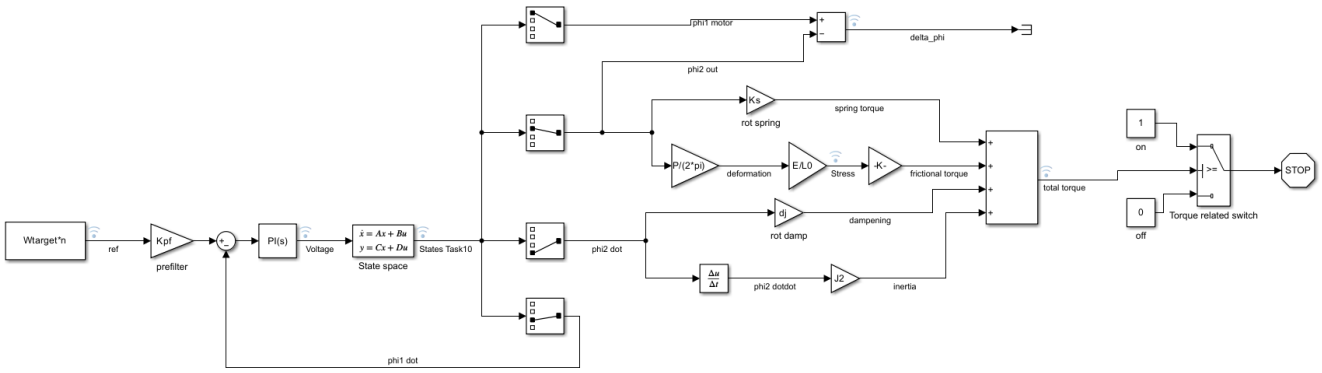

Figure 25: Simulink model of the system based on State-space representation with addition of torsional spring and dampening, Coulomb's friction and inertia

11 Task 11

This section aims to determine the energy consumption of the nut runner during the complete tightening process of an M8 nut. It also aims to calculate how many nuts can be feasibly tightened using a 2,5 Ah battery.

By rewriting Equation (17), the current $i(t)$ can be represented as shown in Equation (53):

$$i(t) = \frac{V(t) - K_e\dot{\varphi}_1(t)}{R} \tag{52}$$

The power $P(t)$ can then be expressed as per Equation (53)

$$P(t) = \frac{V(t) - K_e\dot{\varphi}_1(t)}{R}V(t) \tag{53}$$

Integrating this expression over the clamping time $t_0 - t_1$ gives the total amount of electrical energy supplied to the motor in units of Ws. Dividing this by 3600 gives the total energy supplied E in units of Wh, as per Equation (54).

$$E = \frac{1}{3600}\int_{t_0}^{t_1} \frac{V(t) - K_e\dot{\varphi}_1(t)}{R}V(t)\,dt \tag{54}$$

By plotting the integrated and scaled value over the clamping phase, as shown in Figure 26, the energy consumed during one clamping can be derived.

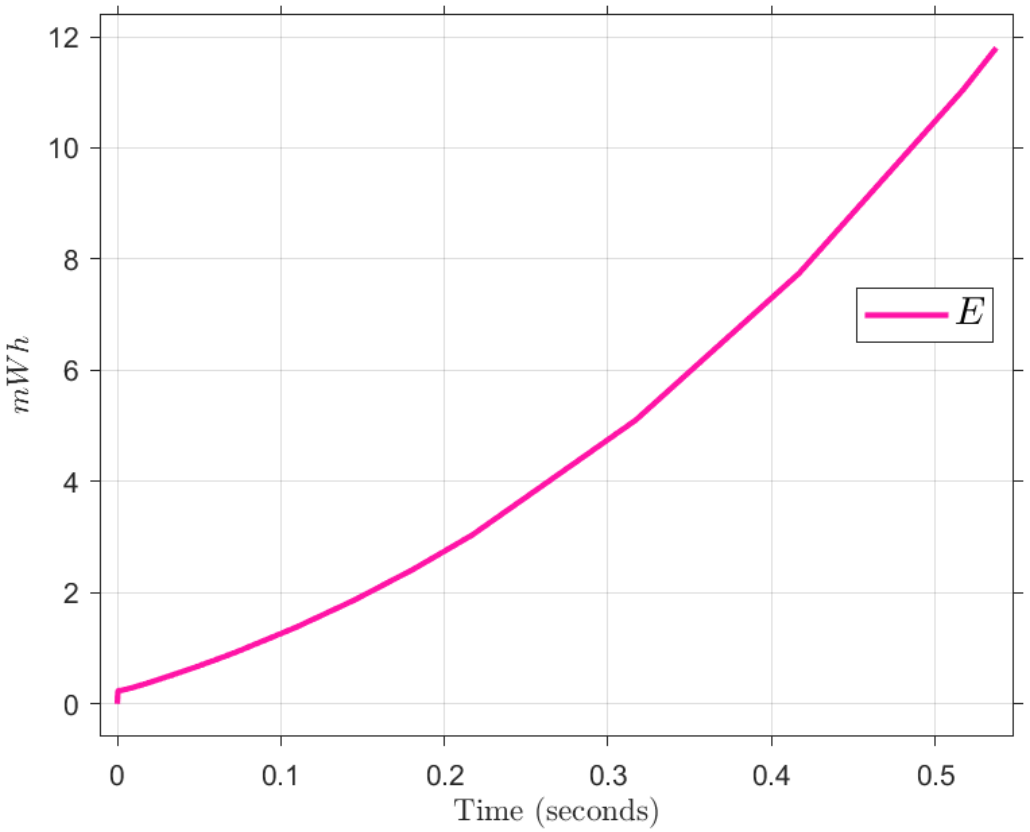

Figure 26: Plot showing the energy E supplied to the motor during the clamping phase, total energy supplied is 11,8mWh

Assuming that the rundown and alignment phase energy consumption is equal to the energy consumed during the clamping phase. Since the nut runner is powered by a 2.5 Ah, 24 V battery, the

total number of nuts tightened n_n with one fully charged battery is estimated to be 2542 nuts as per Equation (55).

$$n_n = \frac{24 * 2.5}{2E} \tag{55}$$

Appendix

Motor data sheet

FAULHABER

Brushless DC-Servomotors 190 mNm

2 Pole Technology 232 W

Series 4490 ... B

Values at 22°C and nominal voltage		4490 H	024 B	036 B	048 B	
1 Nominal voltage	U_N		24	36	48	V
2 Terminal resistance, phase-phase	R		0,22	0,44	0,7	Ω
3 Efficiency, max.	$\eta_{max.}$		87	87	87	%
4 No-load speed	n_0		9 700	10 400	10 800	min⁻¹
5 No-load current, typ. (with shaft ø 6 mm)	I_0		0,527	0,397	0,317	A
6 Stall torque	M_H		2 635	2 760	2 978	mNm
7 Friction torque, static	C_0		4,96	4,96	4,96	mNm
8 Friction torque, dynamic	C_V		7,72·10⁻⁴	7,72·10⁻⁴	7,72·10⁻⁴	mNm/min⁻¹
9 Speed constant	k_n		395	283	220	min⁻¹/V
10 Back-EMF constant	k_E		2,53	3,54	4,56	mV/min⁻¹
11 Torque constant	k_M		24,2	33,8	43,5	mNm/A
12 Current constant	k_I		0,041	0,03	0,023	A/mNm
13 Slope of n-M curve	$\Delta n/\Delta M$		3,6	3,7	3,5	min⁻¹/mNm
14 Terminal inductance, phase-phase	L		73	142	235	µH
15 Mechanical time constant	τ_m		4,9	5	4,8	ms
16 Rotor inertia	J		130	130	130	gcm²
17 Angular acceleration	$\alpha_{max.}$		203	212	229	·10³rad/s²
18 Thermal resistance	R_{th1} / R_{th2}	0,96 / 3,9				K/W
19 Thermal time constant	τ_{w1} / τ_{w2}	23 / 1 222				s
20 Operating temperature range:						
– motor		-30 ... +125				°C
– winding, max. permissible		+125				°C
21 Shaft bearings		ball bearings, preloaded				
22 Shaft load max.:						
– with shaft diameter		6				mm
– radial at 3 000 min⁻¹ (5 mm from mounting flange)		113				N
– axial at 3 000 min⁻¹ (push only)		45				N
– axial at standstill (push only)		135				N
23 Shaft play:						
– radial	≤	0,015				mm
– axial	=	0				mm
24 Housing material		aluminium, black anodized				
25 Mass		742				g
26 Direction of rotation		electronically reversible				
27 Speed up to	$n_{max.}$	18 000				min⁻¹
28 Number of pole pairs		1				
29 Hall sensors		digital				
30 Magnet material		NdFeB				
Rated values for continuous operation						
31 Rated torque	M_N		148	139	137	mNm
32 Rated current (thermal limit)	I_N		7,45	5,06	3,91	A
33 Rated speed	n_N		9 650	10 470	10 930	min⁻¹

Note: Rated values are calculated with nominal voltage and at a 22°C ambient temperature. The R_{th2} value has been reduced by 25%.

Note:

The diagram indicates the recommended speed in relation to the available torque at the output shaft for a given ambient temperature of 22°C.

The diagram shows the motor in a completely insulated as well as thermally coupled condition (R_{th2} 50% reduced).

The nominal voltage (U_N) curve shows the operating point at nominal voltage in the insulated and thermally coupled condition. Any points of operation above the curve at nominal voltage will require a higher operating voltage. Any points below the nominal voltage curve will require less voltage.

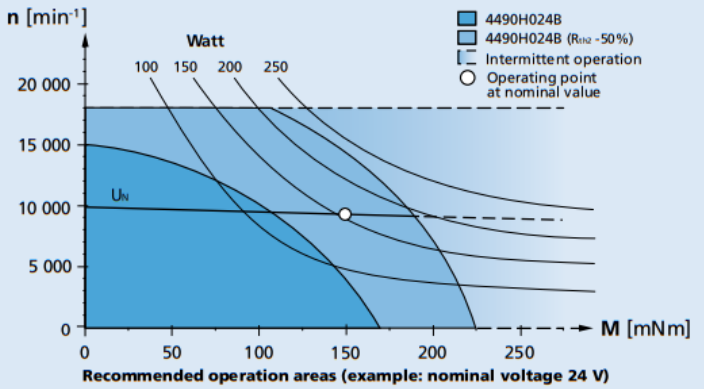

Recommended operation areas (example: nominal voltage 24 V)

For notes on technical data and lifetime performance refer to "Technical Information".

Edition 2023 Nov. 27

www.faulhaber.com

Dimensional drawing

Scale reduced

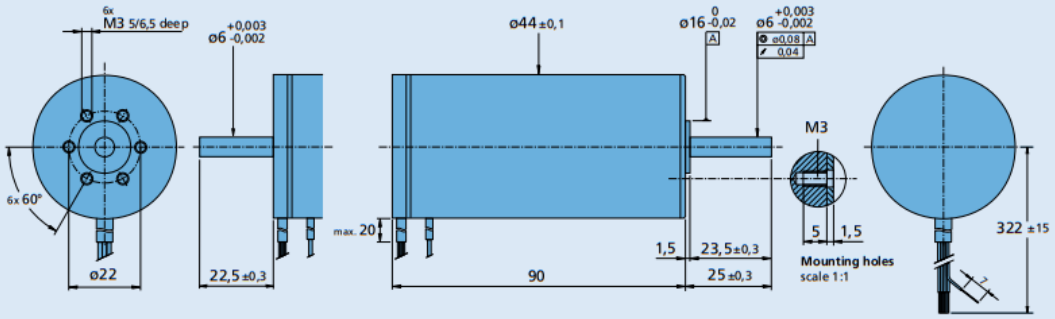

4490 H ... B - K312 **4490 H ... B**

Option, cable and connection information

Example product designation: **4490H024B-K1155**

Option	Type	Description
K1155	Controller combination	Analog Hall sensors for combination with Speed Controller SC or Motion Controller MC
K1026	Sensorless	Motor without Hall sensors
K1838	Encoder combination	Motor with rear end shaft for combination with Encoder IE3
K312	Encoder combination	Motor with rear end shaft for combination with Encoder HEDS/HEDL/HEDM
K3051	Encoder combination	Motor with rear end shaft for combination with Encoder AES
K179	Bearing lubrication	For vacuum of 10^{-5} Pa @ 22°C

Connection

Function	Colour
Phase C	yellow
Phase B	orange
Phase A	brown
GND	black
U_{DD} (+5V)	red
Hall sensor C	grey
Hall sensor B	blue
Hall sensor A	green

Standard cable

Single wires, material PTFE
AWG 16: Phase A/B/C
AWG 26: Hall A/B/C, U_{DD}, GND

Product combination

Precision Gearheads / Lead Screws	Encoders	Drive Electronics	Cables / Accessories
42GPT 44/1	HEDS 5500 IE3-1024 IE3-1024 L HEDL 5540 AEMT-12/16 L AES-4096 L	SC 5004 P SC 5008 S MC 5010 S	MBZ To view our large range of accessory parts, please refer to the "Accessories" chapter.

For notes on technical data and lifetime performance refer to "Technical Information".

Edition 2023 Nov. 27

www.faulhaber.com